Two-dimensional modeling of heat transfers in a ventilated test cell built with various local materials.

ABSTRACT

The main objective of this work is to find a material that attenuates heat transfer and provides an acceptable indoor environment in the habitat of countries with a hot and dry climate like Burkina Faso. The absence of thermal regulations in Burkina Faso leads to the development of buildings constructed with materials that do not provide thermal comfort. This study therefore aims to compare the thermal performance of local materials such as BLT, BTC, concrete block and adobe in order to propose a material adapted to the hot climate. In this work, a modelling and simulation is conducted with the COMSOL software. The modelling is done on a building of dimensions 4m×3m×3m, built successively with cut laterite block (BLT), compressed earth block (BTC), hollow concrete block, and adobe. As for the simulation, it concerns the evolution of the internal and external temperature of the building. The heat flows on the Northern and Southern sides are neglected due to the overhang of the roof. The results obtained show that the cell built with BTC allows a 4°C reduction, the one built with BLT a 2°C reduction and the one built with adobe a 1.5°C gain compared to the one built with concrete block. Thus, the material that best meets the criteria is BTC.

Keywords: Thermal comfort, modeling, simulation, COMSOL, BLT, BLT, adobe.

Nomenclature

Symbols	Désignations	Units
Q	Heat flux	W/m^2
q	Heat flow by conduction	W/m^2
$q^{'}$	Heat flow by radiation in air	W/m^2
C_P	Specific heat	$J/kg.K$
E	Thermal Effusivity	$J/m^2 Ks^{-1/2}$
h	Convective heat transfer coefficient	$W/\mathrm{m}^2.K$
T	East wall temperature	K
T_2	West wall temperature	K
T_3	Roof temperature	K
T_4	Cell air temperature	K
a	Diffusivity	m^2/s
p	Pressure	Pa
t	Time	s
I	Unit tensor	Pa
G	Solar flux arriving on the external faces of the cell	W/m^2
U	Air velocity	m/s

UNDER PEER REVIEW

F	Volume force	N/m^3
u	Component of the velocity field following x	m/s
v	Component of the following velocity field y	m/s

Indices

rad.	Radiation
ex.	External
In.	Internal

Greek symbols

Symbols	Designations	Units
λ	Thermal conductivity	$W/m.K$
ρ	Density	kg/m^3
ε	Emission factor or emissivity of the material	
μ	Dynamic viscosity	$Pa.s$
α	Absorption coefficient	
σ	Stefan-Boltzmann constant	$W/m^2.K^4$
τ	Viscous stress tensor	Pa

UNDER PEER REVIEW

INTRODUCTION

The first international conference on environment held in Stockholm in 1972 was the symbol of global awareness on the depletion of energy resources. The various crises experienced by systems which dependent on fossil fuels, coupled with the rise in fossil oil price and its depletion as well as climate change call for the establishment of a global management policy to manage the planet and its ecosystem. Controlling energy consumption is becoming necessary in all the consumption sectors and notably in building industry. Building sector is one of the largest consumers of energy, nearly 40% of total global energy consumption, and a major factor of greenhouse gas releases (around 35% compared to the other sectors) **[1]**. Burkina Faso is a country with a dry tropical climate characterized by high temperatures (which can reach 40° C to 45° C) for which building models require cooling systems that results in high energy consumption. The energy consumption of buildings in the public administration, notably due the use of air condition equipment (air conditioners, fans, etc.) is estimated at 30,000 MWh / year. The financial cost of this consumption is estimated at CFA F 3.4 billion/ year **[2]**.

Energy consumption in terms of electricity for air condition only represents 30 to 70% of the total consumption of the population **[3]**. According to consumers, air condition is therefore one of the most effective alternatives for maintaining an acceptable atmosphere in buildings. This leads to overbilling, overconsumption of energy in buildings and irregular supply of electricity. This is partly due to the lack of thermal regulation in the building industry and the fact of not taking energy into consideration in the designing of buildings. It is therefore necessary to promote energy efficiency in buildings.

In addition, it would be advisable to offer new construction systems which promote materials that take thermal comfort into account, reduces electricity bills and CO_2 releases in the environment. According to, thermal comfort can be achieved by a judicious choice of building materials and a good architectural policy **[4]**.

It is in the context of improving thermal comfort in a building that our study focuses on the theme: **Two-dimensional modeling of heat transfers in a ventilated test cell, built from various local materials.**
In this study, heat performances of the various local materials used for construction will be compared in order to find a typical material adapted to our climatic condition.

MATERIALS AND METHODS

1. Description of the physical method

The modeling of heat transfers in a building is very complex. Indeed, it is necessary to couple heat transfers by radiation, by convection and by conduction with mass transfers when they exist. To simplify the study, a physical model in 2D of the cell will be adopted by neglecting the releases from the lowest radiation, particularly on the Northern and Southern sides which are also supposed to receive the incident solar radiation due the roof overhangs as shown in **figure 1.** The physical model of the test cell is shown in **figure 2.** It is a living cell of 3 m high and 3 m wide. The Western, Eastern walls and the roof are 10 cm thick. The terrace is 20 cm thick. The cell has two openings. A first opening of 0.1 m × 0.2 m in the wall enabling the entry of fresh air into the test cell. A second opening of 0.1 m × 0.2 m in the Western wall allows hot air to escape. Heat exchanges between the building and the external environment as well as the exchanges inside the cell are also shown in **figure 2.**

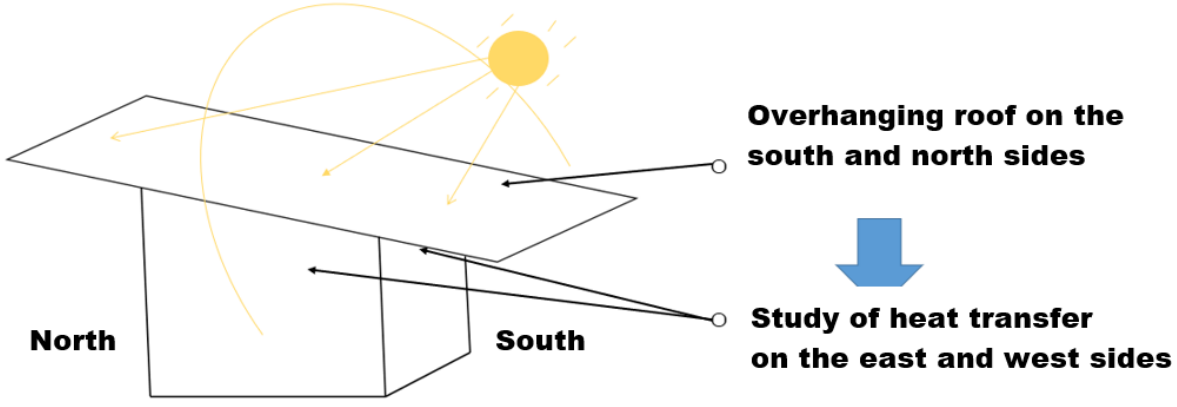

Figure 1: Perspective view

UNDER PEER REVIEW

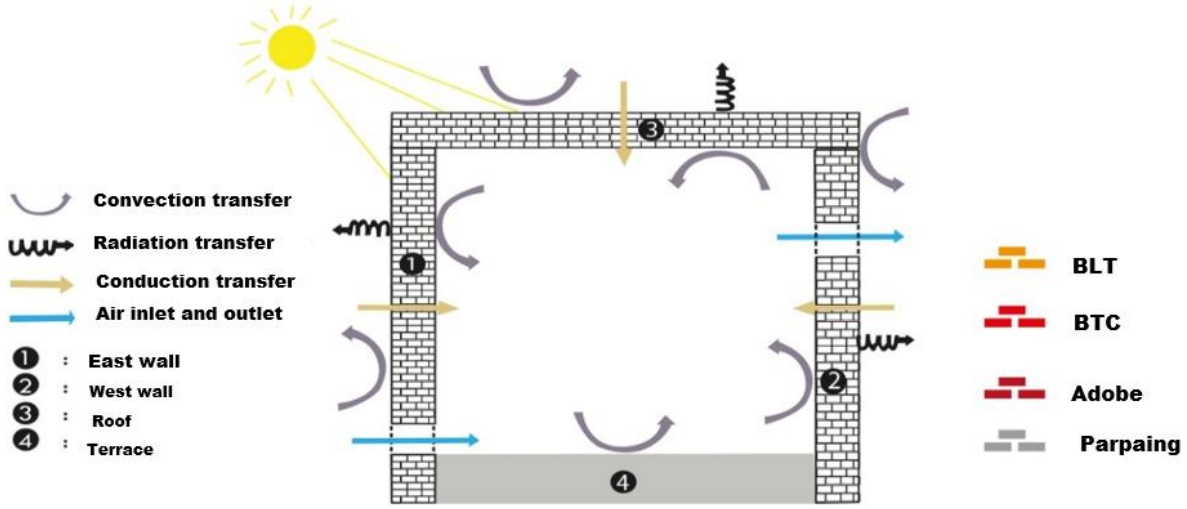

Figure 2: Geometric model showing heat exchanges

2. Materials and descriptions

The dimensions of the cell introduced with COMSOL enabled to obtain the physical model in **figure 3**. COMSOL is a simulation Software which equations are discretized by the finite element method and enables to solve any type of problem that can be described by partial differential equations **[5]**. COMSOL Software provides automatic and semi-automatic 1D, 2D, and 3D meshing tools with user-controlled parameters. It has finite elements of various shapes (tetrahedral, prismatic, hexahedral or triangular, etc.) and orders (linear, quadratic, etc.). **Figure 4** shows the mesh of the model. The mesh of our field of study is triangular. It has 1661 elements and 7246 resolved degrees of freedom. The mesh area is 8.7 m^2.

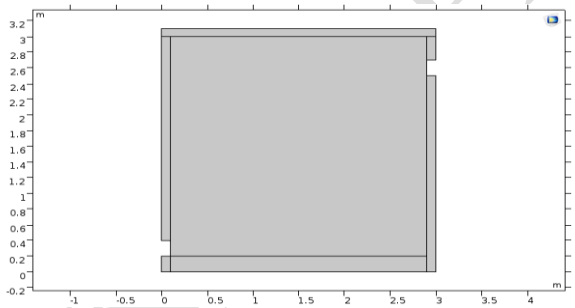

Figure 3: Physical model conceived with COMSOL

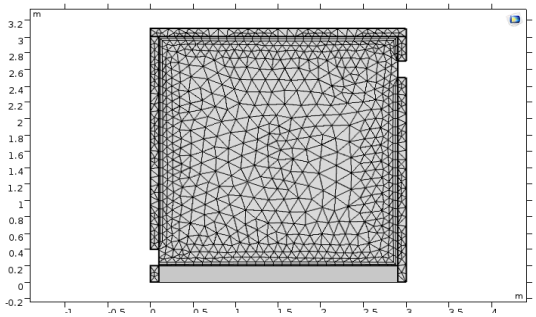

Figure 4: Meshing of the geometric model

3. Mathematic model of heat and air transfers

The heat and air transfer equations are obtained with the COMSOL software after the definition of the physical model; (COMSOL Multiphysics reference manual) **[6]**; the book (the book heat transfer handbook) **[7]**; (M. Veera Krishna and al., 2020) **[8]**; (M. Veera Krishna and al., 2018) **[9]**; (L. Chen and al., 2017) **[10]**.

3.1. Basic equations of heat and air transfers

UNDER PEER REVIE

The equation ruling heat transfer in solids is given by equations **(1)**:

$$\rho.C_p \frac{\partial T}{\partial t} + \rho C_p \,\mathrm{U}.\nabla T + \nabla.\mathrm{q} = Q_{rad} \textbf{ (1)}$$

With: $q = -\lambda(\nabla.\nabla T)$ **(2)**; $Q_{rad} = \alpha G$ **(3)** the term showing heat transfer by radiation. is the velocity field defined by the translational motion of the solid as the solid moves. n our case of study, the solid is immobile so $U = 0m/s$. Equation **(1)** then becomes:

$$\rho.C_p \frac{\partial T}{\partial t} + \nabla.q = Q_{rad} \textbf{ (4)}$$

The general heat transfer equation in the fluid is given by the equation **(5):**

$$\rho.C_p \frac{\partial T}{\partial t} + \rho C_p U.\nabla T + \nabla.(q + q'_{rad}) = -\frac{1}{\rho}\frac{\partial \rho}{\partial T} T(\frac{\partial P}{\partial t} + U.\nabla P) + \tau : \nabla U + Q_V \qquad \textbf{(5)}$$

We assume that the air flow in the cell is incompressible. The work of the pressure forces is then zero and $\nabla(U) = 0$. The radiation inside the cell is neglected so $q_{rad} = 0$ et $Q_V = 0$ as there are no volume sources of heat production in the cell. Aking these three assumptions into account, equation **(5)** becomes : $\rho.C_p \frac{\partial T}{\partial t} + \rho C_p U.\nabla T = \nabla.(\lambda \nabla T)$ **(6)**

The equation showing air flow is based on Navier-Stockes equations. Then we have:
$$\rho \frac{\partial U}{\partial t} + \rho(U.\nabla)U = \nabla.[-pI + \mu(\nabla U + (\nabla U)^T) - \frac{2}{3}\mu(\nabla.U)\,\mathrm{I}] + \mathrm{F} \textbf{ (7)}$$

The continuity equation is given by the equation **(8)**:

$$\frac{\partial \rho}{\partial t} + \nabla(\rho.U) = 0 \qquad \textbf{(8)}$$

The the air flow in the cell is incompressible so the continuity equation becomes: $\nabla(U) = 0$ and equation **(7)** becomes:

$$\frac{\partial U}{\partial t} + \rho(U.\nabla)U = \nabla.[-pI + \mu\nabla U] + \mathrm{F} \qquad \textbf{(9)}$$

F only exists in natural convection, where Boussinesq's approximation assumes that variations in density do not impact the flow field, except the fact that they generate buoyancy forces which are volume forces **[11]**, **[12]**. So the fluid flow equation is:

$$\frac{\partial U}{\partial t} + \rho(U.\nabla)U = \nabla.[-pI + \mu\nabla U] \qquad \textbf{(10)}$$

With I the unit tensor.

3.2. Simplifying assumptions of the model

UNDER PEER REVIEW

The simplifying assumptions about heat transfer and the physical model are as follows :

- Heat exchange is two-dimensional
- The thermophysical properties of building materials are constant. These are thermal conductivity (λ), density (ρ) and heat capacity (C_p) ;
- The celestial vault is assimilated to a black body ;
- The radiation inside the cell is assumed to be neglected;
- Air is homogeneous
- The air flow is laminar ;
- The temperature of the terrace is constant and equal to that of the ground.

3.3. Detailed heat and air transfer equations

The simplifying assumptions applied to the governing equations give the following detailed equations.

The heat transfer equation at the Eastern wall is given by :

$$\rho_{Eastern_{wall}}.Cp_{Eastern_{wall}}\frac{\partial T}{\partial t}-\lambda_{Eastern_{wall}}(\frac{\partial^2 T}{\partial x^2}+\frac{\partial^2 T}{\partial y^2})=\alpha_{Eastern_{wall}}G_{Eastern_{wall}} \quad \textbf{(11)}$$

The heat transfer equation for the Western wall is :

$$\rho_{Western_{wall}}.Cp_{Western_{wall}}\frac{\partial T_2}{\partial t}-\lambda_{Western_{wall}}(\frac{\partial^2 T_2}{\partial x^2}+\frac{\partial^2 T_2}{\partial y^2})=\alpha_{Western_{wall}}G_{Western_{wall}} \quad \textbf{(12)}$$

The equation for heat transfer in the roof is :

$$\rho_{roof}.Cp_{roof}\frac{\partial T_3}{\partial t}-\lambda_{roof}(\frac{\partial^2 T_3}{\partial x^2}+\frac{\partial^2 T_3}{\partial y^2})=\alpha_{roof}G_{roof} \quad \textbf{(13)}$$

The heat transfer equation in air is then :

$$\rho_{air}.Cp_{air}\frac{\partial T_4}{\partial t}+\rho_{air}Cp_{air}(u\frac{\partial T_4}{\partial x}+v\frac{\partial T_4}{\partial y})-\lambda_{air}(\frac{\partial^2 T_4}{\partial x^2}+\frac{\partial^2 T_4}{\partial y^2})= \quad \textbf{(14)}$$

$$h_{east_{wallin.}}(T-T_4)+h_{west_{wallin.}}(T_2-T_4)+h_{roofin.}(T_3-T_4)+h_{terrace}(T_0-T_4)$$

The equation for the air flow in the cell is :

$$\frac{\partial U}{\partial t}+\rho(U.\nabla)U=\nabla.[-pI+\mu\nabla U]+\mathrm{F} \quad \textbf{(15)}$$

Since convection is forced, the volume forces are negligible. The result is :

$$\rho_{air}\frac{\partial U}{\partial t}+\rho_{air}(U.\nabla)U=\nabla.(-pI) \quad \textbf{(16)}$$

Along the x axis, we have :

$$\rho_{air}(\frac{\partial u}{\partial t}+u\frac{\partial u}{\partial x}+v\frac{\partial u}{\partial y})=-\frac{\partial P}{\partial x}+\mu_{air}(\frac{\partial^2 u}{\partial x^2}+\frac{\partial^2 u}{\partial y^2}) \quad \textbf{(17)}$$

Along the y axis, we have :

$$\rho_{air}(\frac{\partial v}{\partial t}+u\frac{\partial v}{\partial x}+v\frac{\partial v}{\partial y})=-\frac{\partial P}{\partial y}+\mu_{air}(\frac{\partial^2 v}{\partial x^2}+\frac{\partial^2 v}{\partial y^2}) \quad \textbf{(18)}$$

3.4. Initial conditions

The initial conditions are recorded in Table 1 :

Table 1 : Initial values entered

Components	Initial values

UNDER PEER REVIEW

Wall temperature	303 K
Indoor air temperature	303 K
Outside air temperature	303 K
Roof temperature	303 K
Soil temperature	303 K
Air pressure at the inlet	$0Pa$

3.5. Boundary conditions

The ambient air temperature (Tam) and the solar flux (G), arriving on the external faces of the cell walls, used for the simulation, are those of the weather data of the city of Ouagadougou for the typical day of April of the year 2019.

3.5.1. Boundary conditions on the external faces of the walls

The external faces of the cell walls are subject to convection and solar radiation. The boundary conditions on the external faces are given by :

- External face of the Eastern wall (x= 0 ; y ; t)

$$\lambda_{Estern_{wall}}.\nabla T = \alpha_{Estern_{wall}}.G_{Estern_{wall}} + h_{Estern_{wall_{ex}}}(T_{amb} - T) + \varepsilon_{Estern_{wall}}(G_{Estern_{wall}} - \sigma.T^4) \quad \textbf{(19)}$$

- External face of the Western wall (x= 0 ; y ; t)

$$\lambda_{Western_{wall}}.\nabla T_2 = \alpha_{Western_{wall}}.G_{Western_{wall}} + h_{Western_{wall_{ex}}}(T_{amb} - T_2) + \varepsilon_{Western_{wall}}(G_{Western_{wall}} - \sigma.T_2^4) \quad \textbf{(20)}$$

- External face of the roof (x ; y=3 ; t)

$$\lambda_{roof}.\nabla T_3 = \alpha_{roof}.G_{roof} + h_{roof_{ex}}(T_{amb} - T_3) + \varepsilon_{roof}(G_{roof} - \sigma.T_3^4) \quad \textbf{(21)}$$

3.5.2. Boundary condition on the internal faces

The internal faces of the cell walls are subject to convection. The boundary conditions on the inner faces of the cell walls are given by the equations (15) ; (16) ; (17) :

- Internal face of the Eastern wall (x=0.1 ; y ; t)

$$\lambda_{Estern_{wall}}.\nabla T_4 = h_{Estern_{wall_{in}}}(T - T_4) \quad \textbf{(22)}$$

- Internal face of the Western wall (x=2.8 ; y ; t)

$$\lambda_{Western_{wall}}.\nabla T_4 = h_{Western_{wall_{in}}}(T_2 - T_4) \quad \textbf{(23)}$$

- Internal face of the roof (x ; y=3 ; t)

$$\lambda_{roof}.\nabla T_4 = h_{roof_{in}}(T_3 - T_4) \quad \textbf{(24)}$$

3.5.3. Boundary conditions on opening 1 (the air inlet)

$$U = U_0 \quad \textbf{(25)}$$

3.5.4. Boundary conditions on opening 2 (air outlet)

$$P = 0 \quad \textbf{(26)}$$

3.6. Résolution

The numerical solution of the established equations is made possible by a calculation code designed in the COMSOL software. The physical model defined in the COMSOL software allows to obtain

UNDER PEER REVIEW

equations (11), (12), (13), (14) and (16). These equations and their associated boundary and initial conditions are solved by the COMSOL software using finite element discretization.

3.7.Thermophysical properties and entry parameters

The thermophysical properties of the materials used are in **Table 2.**

BLT**:** Cute Laterite Block
BTC: Compressed Earth Block.

For digital simulation, there are four subdomains which are the Western wall, the Eastern wall, the roof, and the indoor air. The model used is the general heat transfer model. The **table 3** gives the input parameters taken into account in the simulation**:**

Table 2: Thermophysical Properties ([13] ; [14] ; [15] ; [16])

Property / Material	Thermal conductivity (λ) (W/m K)	Volume mass (ρ) (kg/m^3)	Thermal capacity (C_p) (J/kg K)	Diffusivity (a) (m^2/s)	Effusivity E (J/m^2 K s$^{-0,5}$)
Concrete	1.800	2300	880	8.9×10^{-7}	1908
Concrete blocks	0.670	1250	880	6.7×10^{-7}	858
BLT	0.469	1853	928	2.7×10^{-7}	898
BTC	0.671	1960	1492	2.3×10^{-7}	1401
Adobe	0.450	1394	1213	2.7×10^{-7}	872

Table 3: Input Parameters

Parameters	Values
Wall height (m)	3
Wall thickness (m)	0.1
Roof thickness (m)	0.1
Roof length (m)	3
Terrace thickness (m)	0.2
Terrace length (m)	2.8
Input air velocity (m/s)	0.294
Input air pressure (Pa)	0 Pa
Convection coefficient of the external side of the Eastern wall (W/m^{2}K)	16.16
Convection coefficient of the internal side of the Eastern wall (W/m^{2}K)	4
Convection coefficient of the external side of the Western wall (W/m^{2}K)	16.16
Convection coefficient of the internal side of the Western wall (W/m^{2}K)	4
Convection coefficient of the external side of the roof (W/m^{2}K)	16.16

UNDER PEER REVIEW

Convection coefficient of the internal side of the roof (W/m^2K)	4
Convection coefficient of the internal side of the floor(W/m^2K)	2

RESULTS AND DISCUSSION

1. Evolution of temperature, speed and pressure: case of the cell built in BLT

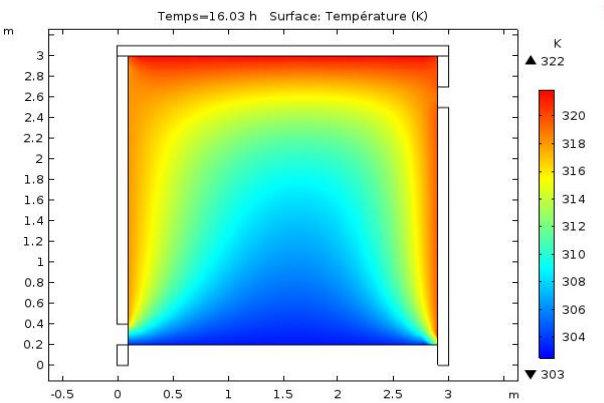

Figure 5: Surface temperature of the cell

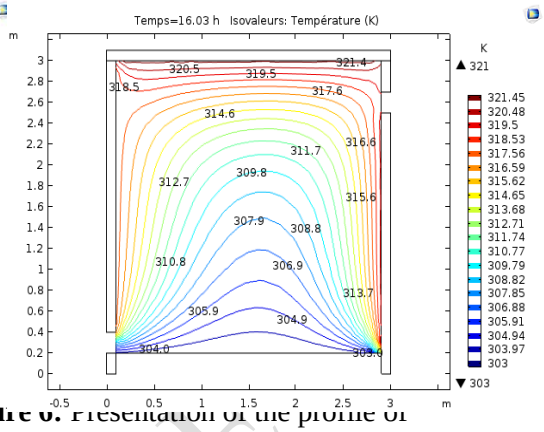

Figure 6: Presentation of the profile of the cell temperature iso-values

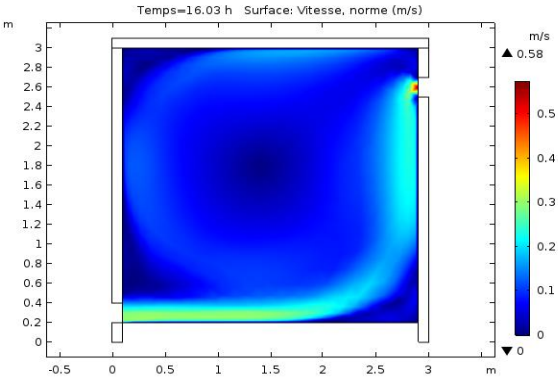

Figure 7: Evolution of the air speed in the cell

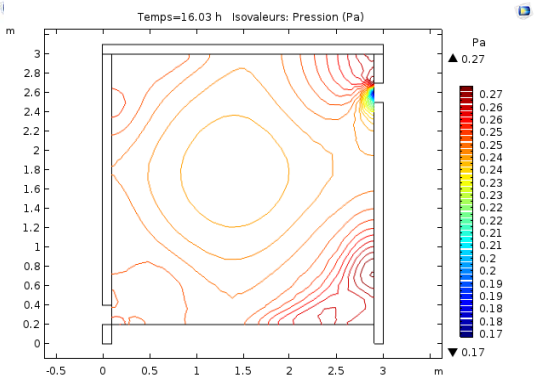

Figure 8: Pressure iso-values in the cell

1.1. Surface temperature

These surfaces enable to determine the temperatures at any point in the cell. They are shown in Figures 5 and 6. High temperature values are recorded near the internal sides of the walls and the roof. Temperature distribution in the center and towards the floor of the cell shows that the temperature is lower in this part of the cell. High temperatures recorded on the internal surfaces are due to the solar radiation received by the walls and the roof during daytime. The walls and the roof will then release heat by conduction contributing therefore to their heating. The heat is then transferred to the cell by convection heating the cell. Low temperatures recorded in the center and at a low height are due to the air flow through the openings.

1.2. Temperature iso-values

Isothermal curves or temperature iso-values are distinguished by their colors and are shown in figure 6. Isothermal curves are very dense near the internal sides of the walls and the roof. This means that high temperature fluctuations are recorded around the internal walls. In the center of the cell and for low heights, the isothermal lines are less dense and much disparate. Temperatures at this level of the cell are lower and vary very little.

UNDER PEER REVIEW

1.3. Speed surfaces

Figure 7 shows the evolution of the air speed inside the cell within a day. The air flow speed inside the room near the openings is high and remains low within the rest of the cell. Speed has little impact on internal temperature. Convection due to air flow is then very weak. The high velocity values observed at the opening which constitutes the exit of the air are due to the low air pressure values recorded in this opening.

1.4. Pressure iso-values

Figure 9 shows the pressure field in the cell. Pressure lines have almost the same colors, therefore nearly the same value except in the exit. There is a slight variation of pressure.

2. Comparative study of temperature evolution in the cell built in BLT, BTC, concrete blocks and in adobe.

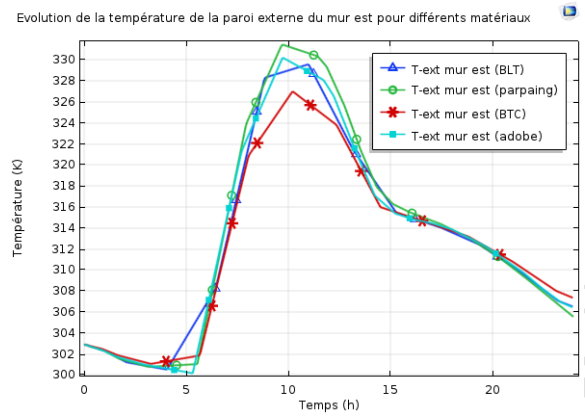

Figure 9 : Temperature evolution of the external wall of the Eastern wall made of BLT, BTC, concrete block and adobe

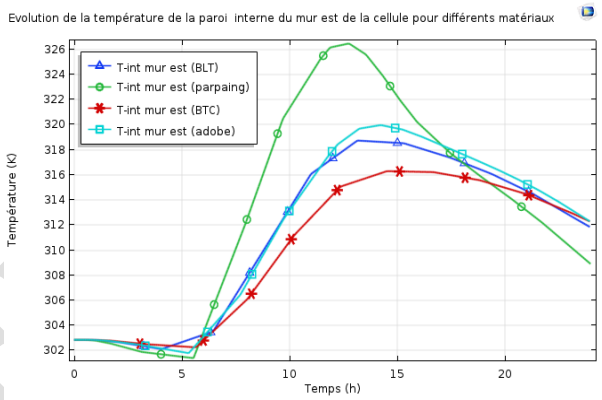

Figure 10 : Evolution of the temperature of the internal wall of the Eastern wall made of BLT, BTC, concrete block and adobe

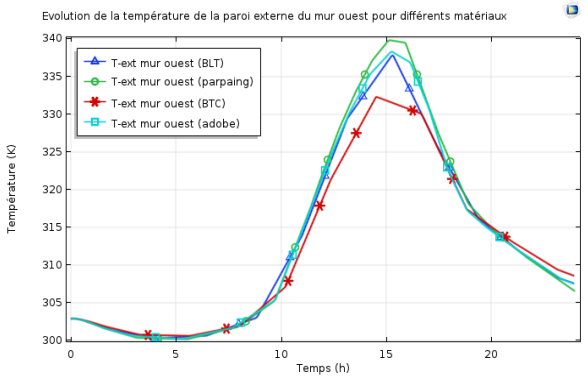

Figure 11: Temperature evolution of the external wall of the Western wall in BLT, BTC, concrete block and adobe

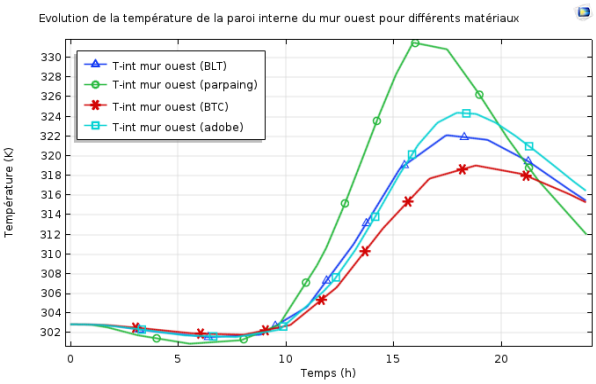

Figure 12 : Temperature evolution of the internal wall of the Western wall made of BLT, BTC, concrete block and adobe

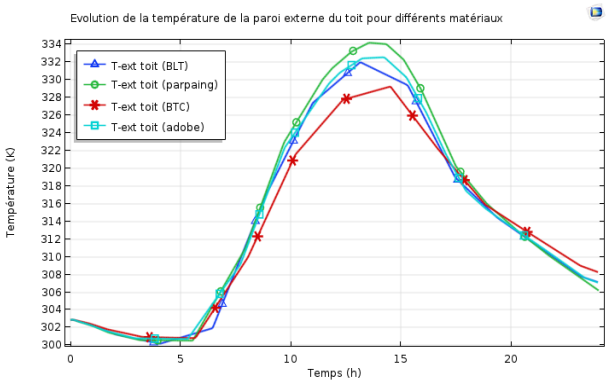

Figure 13 : Evolution of the temperature of the external wall of the BLT, BTC, concrete block and adobe roof

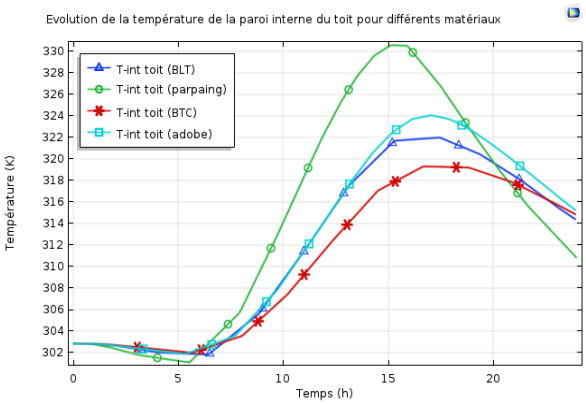

Figure 14 : Evolution of the temperature of the internal wall of the BLT, BLT, concrete block and adobe roof

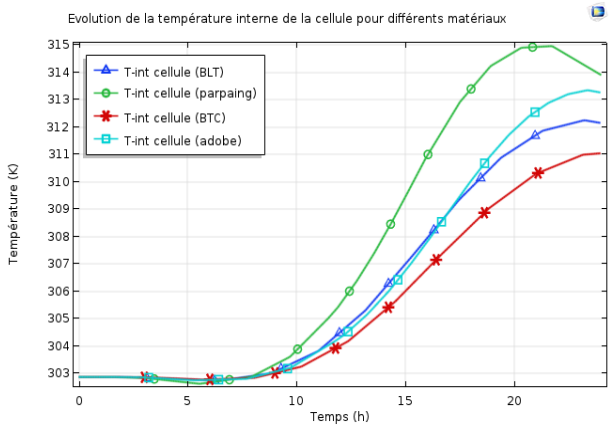

Figure 15 : Evolution of the internal temperature of the cell

UNDER PEER REVIEW

2.1. Evolution of the temperature of the external side of the Western wall

Figure 9 shows the temperature evolution of the external surface of the Eastern wall of the cell built in BLT, BTC, concrete blocks and adobe. It shows that the temperature trends of the external side of the Eastern wall are the same. Maximum temperatures are reached between 9 a.m. and 11 a.m. This period is when the Eastern wall is most exposed to the sun. It should be noted that BLT, BTC and adobe have 3°C, 5 °C and 2 °C, respectively lower than concrete blocks. Temperature differences are not very high but BTC and BLT have larger differences. This means that the effusivity of these materials is higher than that of concrete blocks. Indeed, the effusivity of the concrete blocks is low (858 J / $m^2s^{-0.5}$) contributing to quickly heat its surface unlike BTC, BLT and adobe which respectively have the following effusivities: 1400 J / $m^2s^{-0.5}$; 898 J / $m^2s^{-0.5}$; 872 J / $m^2s^{-0.5}$ which surface get heated less quickly.

2.2. Evolution of the temperature of the internal side of the Eastern wall

Figure 10 shows temperature evolution of the internal surface of the Eastern wall of the cell built with BLT, BTC, concrete block and adobe. A decrease in the temperature of the internal wall for the various materials is noticed all the night long. In the daytime, the temperature of the internal surfaces increases from 6 a.m. to 11 a.m. and decreases from 11 a.m. to 6 p.m. At night, the internal temperature decreases considerably. The temperature difference of the internal surfaces of the Eastern wall in concrete block and the Eastern wall in BTC, BLT and adobe are 7.5 °C, 10.5 °C and 6.5 °C, respectively. A temperature gain is then recorded for BLT, BTC and adobe compared to the concrete blocks and are 7.5 °C; 10.5 °C and 6.5 °C, respectively. The best gain is recorded with BTC. It should

be noted that the temperature of the internal side of the Eastern wall in concrete blocks highly increases between 6 a.m. and 11 a.m. and decreases suddenly until 24 hours when the value is 307 K or 34 °C. Heat transfer by radiation and by conduction through materials causes an increase in the temperature of the internal side of the Eastern wall for all the materials. In the second half of the day, the Eastern wall no longer receives sunlight, which leads to the decrease in temperature for all the materials. At night, the heat stored during the day is discharged by conduction outside; therefore, the temperature at night decreases. The high temperature gaps between concrete blocks and the other materials are due to the fact that BTC, BLT and adobe have this capacity to absorb sudden temperature fluctuations. These materials then have a high thermal inertia compared to the concrete blocks.

2.3. Evolution of the temperature of the external side of the Western wall

The change in the temperature of the external side of the Western wall of the cell built in BLT, BTC, concrete blocks and adobe is shown in Figure 11. The temperatures of the external wall for the various materials decrease all the night long. At daytime, the temperature of the external side increases from 9 a.m. to 3 p.m. and falls from 3 p.m. to 6 p.m. contrary to the temperatures of the external side of the Eastern wall which rises as from 5 a.m. The temperature gap of the external surfaces of the Western concrete blocks wall and the Eastern BLT, BTC and adobe wall are 2.5 °C, 8 °C and 2 °C, respectively. The gaps noticed between the temperatures of the external side of the Western wall are fairly the same as those of the temperatures of the external side of the Eastern wall which are 3 °C; 5 °C and 2 °C, respectively. Temperature gaps for the various materials are not very high, as the change in the external temperature of the Eastern wall. The maximums values of the surface temperature for BTC, BLT and adobe are lower than that of concrete block. Indeed, the effusivity of BTC is higher than that of BLT, adobe and concrete blocks, leading to the external side of BTC to heat less quickly compared to other materials.

2.4. Evolution of the temperature of the external side of the Western wall

Figure 12 shows temperature evolution of the internal side of the Western wall built with various materials including BLT, concrete blocks, BTC and adobe. It should be noted a decrease in the temperature of the internal wall for the various materials throughout the night. This decrease is much higher or even brutal for the temperature of the concrete blocks wall. In daytime, the temperature of the internal side increases from 10 a.m. to 6 p.m. for BLT, BTC and adobe except the temperature of the concrete blocks which starts falling as from 4 p.m. There is a decrease in maximum temperatures of the external side of the Western wall. The temperature gap of the internal sides of the Eastern side of the concrete block wall and the eastern wall in BTC, BLT and adobe are 10 °C, 13 °C and 7.5 °C, respectively. The sudden increase in temperature of the concrete blocks wall is due to its thermal inertia. The thermal inertia of the concrete block is lower than that of the other three materials, thus causing a strong variation in the temperature of the internal side. BTC, BLT and adobe contain temperature variation better and this is due to their thermal inertia, which is fairly higher than that of concrete blocks. The temperature increase for materials is due, on the one hand, to heat received by convection within the cell and on the other hand, by conduction through the wall of the solar flow received during daytime. The decrease in temperature is due to the rejection of heat stored during the daytime by conduction through the wall and by convection.

2.5. Evolution of the temperature of the external wall of the roof

Figure 13 shows the evolution of the temperature of the external wall of the cell roof built in BLT, BTC, concrete blocks and adobe. In daytime, temperatures rise as early as 5 a.m. and gets to its peak between 1 p.m. and 3 p.m. and then begin to decrease for the rest of the day. At night, there is a significant decrease in temperature for the various materials used. It should be noted that BTC, BLT and Adobe have 2 °C; 5 °C and 1.5 °C, respectively lower than the concrete blocks. The increase in the temperature of the external side of the roof at a precise period of the day is due to the large solar flow received during the day. Temperature gaps are due to material effusivity. Concrete blocks have,

UNDER PEER REVIEW

in fact, a lower effusivity than that of BTC, BLT and adobe as shown in table 1. Thus, the surface temperature of the concrete blocks grows faster and reaches its peak before the three other materials.

2.6. Evolution of the temperature of the internal wall of the roof

Figure 14 shows the change in the temperature of the internal side of the roof built with different materials such as BLT, concrete blocks, BTC and Adobe. It was noticed that the temperature of the concrete blocks roof is less stable than that of the BLT, BTC and adobe roof. The temperature of the internal wall for the various materials during the whole night decreases considerably. This decrease is most noticeable for the temperature of the concrete blocks wall. Daytime is characterized by large variations in the temperature of the internal side. In daytime, the temperature increases from 6 a.m. to 5 p.m. for BLT, BTC and adobe except the temperature of the concrete blocks which starts falling from 4 p.m. The temperature gap of the internal surfaces of the Eastern concrete blocks wall and the Eastern BLT, BTC and adobe wall are 9 °C; 12 °C and 7 °C, respectively. BLT and BTC have virtually the same gap and show lower temperatures. Yet, the Adobe has its maximum temperature closer to that of the concrete block. The increase in the internal temperature of the roof during the day is due to the fact that the roof is exposed to solar flow throughout the day. Heat reaches the internal surface by conduction through the roof. The decrease in temperature towards the end of the day and at night is due to the release of heat from the inside to the outside of the cell by conduction through the roof and the lack of sunlight at night. The sudden rise and the rapid decrease in temperature of the internal side of the concrete blocks compared to BTC, BLT and adobe seems to be due to the thermal inertia of the concrete blocks which is lower than that of other materials. Concrete blocks poorly contain heat conduction leading to the overheating of the internal surface and the sudden fall in the temperature of the internal surface. The temperature of the internal side of the BTC roof is the most stable followed by that of BLT and adobe. Indeed BTC, BLT and adobe used have a higher thermal inertia compared to the concrete blocks, giving them this capacity to absorb these thermal losses.

2.7. Evolution of the internal temperature of the cell

The Figure 15 shows the evolution of the internal temperature of the cell built with BLT, BTC, concrete blocks and adobe. It should be noted that the temperature of the concrete block cell is higher than the temperature of the cell in BLT, BTC and adobe. Regardless of the type of material, the internal temperature of the cell for different materials increases throughout the day and for one part of the night. For the rest of the night, the internal temperature falls. The maximum temperature gaps of the cell in BLT, BTC and adobe as compared to concrete blocks are 2.5 °C; 4 °C and 1.5 °C, respectively. Temperature gaps are slight but BLT and BTC have almost the same gap and have lower temperatures. The increase in the internal temperature of the cell constructed with BLT, BTC, adobe and concrete blocks is due to the transfer of heat from outside to inside of the cell during daytime. The diffusivity of concrete blocks ($6.1.10^{-7}m^2$ / s) is high compared to those of BTC ($2.3.10^{-7}m^2$ / s), BLT ($2.7.10^{-7}m^2$ / s) and adobe ($2.7.\ 10^{-7}m^2$ / s) leading the concrete block to conduct more heat. Thus, concrete blocks get quickly heated. Thermal diffusivity of the other three materials is low, that is why the internal temperature of these materials increases slowly and the cell warms up slowly. The maximum temperature gaps found are due to the thermal properties of the materials used. The thermal inertia of the concrete blocks remains low compared to that of BTC, Adobe and BLT. The concrete blocks weakly contain thermal gains, justifying the sudden fall in temperature and very high temperatures.

CONCLUSION

The simulation of the evolution of the internal temperature of the cell and that of external and internal sides of the Eastern, Western walls and of the roof was made. The study shows that BTC (Compressed Earth Block) is the material that offers lower temperatures (varying between 303 K and 311 K) and a good internal thermal comfort compared to BLT (Cut Laterite Block), concrete blocks and adobe. The temperatures inside the cell built with BLT (varying between 303 K and 312.5 K) and adobe (varying between 303 K and 313.5 K) are lower than those of the cell built with BTC but higher than that of

UNDER PEER REVIEW

concrete blocks (varying between 303 K and 315 K). BTC is the material that best mitigates the transmission of heat from outside to the inside compared to BLT, to the concrete blocks and to adobe. The internal surfaces of the cell constructed with BTC have a temperature that slightly varies from the temperature of the internal surfaces of the cell constructed with BLT, concrete blocks, and adobe. Houses built with mud offer a better indoor thermal environment than those constructed with modern materials more and more used in the construction sector in Burkina Faso.

COMPETING INTERESTS DISCLAIMER:

Authors have declared that no competing interests exist. The products used for this research are commonly and predominantly use products in our area of research and country. There is absolutely no conflict of interest between the authors and producers of the products because we do not intend to use these products as an avenue for any litigation but for the advancement of knowledge. Also, the research was not funded by the producing company rather it was funded by personal efforts of the authors

BIBLIOGRAPHIC REFERENCES

[1] IFDD, Guide to sustainable building in tropical regions. Volume 1: Design strategies new buildings in tropical regions, Institut de la Francophonie et du Sustainable Development, 191 p, 2015.

[2] P. Y. Gagnon and P. H. Nfaoui, "Renewable energies: Distributed and community production, Institut de la Francophonie et du Développement Durable (IFDD), Liaison Energie-Francophonie, Vol. 94, pp. 3–5, 2013.

[3] "National Communication from Burkina Faso, United Nations Framework Convention on Climate Change," p. 132, 2001.

[4] A. Kemajou and L. Mba, "Building materials and thermal comfort in hot zones: application to the case of Cameroonian climatic regions, Rev. renewable energies,Vol. 14 N°2 (2011) pp. 239-248,2011."

[5] M. Mohamed, "Simulation of the effect of inserting turbulators within a fluid flow in a pipe, from the point of view of heat transfer and pressure drop, Master thesis, Merbah-Ourgla University , p.50, 2014. "

[6] COMSOL Multiphysics Reference Manual,2017 : https://doc.comsol.com/5.3/doc/com.comsol.help.comsol/COMSOL_ReferenceManual.pdf

[7] P. Y. Lagrée, Thermal and mass transfers in fluids, ENSTA course, p.24, October 2018.

[8] M. Veera Krishna , N. Ameer Ahamad and Ali J. Chamkha, ''Hall and ion slip impacts on unsteady MHD convective rotating flow of heat generating/ absorbing second grade fluid'', Alexandria Engineering Journal, ,2020, https://doi.org/10.1016/j.aej.2020.10.013.

[9] M. Veera Krishna and Ali J. Chamkha, ''Hall effects on unsteady MHD flow of second grade fluid through porous medium with ramped wall temperature and ramped surface concentration'', American Institute of Physics,2018, https://doi.org/10.1063/1.5025542.

[10] L. Chen, M. Li, M. Ni and N. Zhang, ''MHD effects and heat transfer analysis in magneto-thermo-fluid-structure coupled field in DCLL blanket'', International Communications in Heat and Mass Transfer,2017, https://10.1016/j.icheatmasstransfer.2017.04.009.

[11] A. Bejan and A. D. Kraus, heat transfer handbook, p.408, 2003.

[12] Z. Rida, K. Sofiane, and B. Dadda, "Natural convection in an inclined rectangular cavity of different aspect ratios," Rev. renewable energies, vol. 19, no. 1, pp. 97–109, 2016.

[13] ZOMA Fati, "Experimental study of thermomechanical properties and simulation of the energy performance of composite materials formulated on the basis of clayey earth and plant reinforcements". Doctoral thesis, Joseph Ki-ZERBO University, Ouagadougou, Burkina Faso, p.250, 2016.

[14] IEPF, Energy efficiency of air conditioning in tropical regions, Volume 1: Design of new buildings, 2006.

[15] A. COMPAORE, "Study of the thermal performance of a typical habitat in burkina faso. Application: contribution to the implementation of thermal regulations, Doctoral thesis, Joseph KI-ZERBO University, Ouagadougou, Burkina Faso, p.168, 2018. "

[16] ISSP / UJKZ, "Scientific report, international conference on energy efficiency and thermal

UNDER PEER REVIEW

regulation in buildings, Ouagadougou, Burkina Faso 2015”

UNDER PEER REVIEW